Inorganic Materials and Process for Bioresorbable Electronics

Min-Ho Seo[1], Seongbin Jo[2], and Jahyun Koo[3]

[1] Center for Bio-Integrated Electronics, Northwestern University, Evanston, 60201, USA.
[2] Chemical and Biomolecular Engineering, University of Illinois at Urbana-Champaign, Urbana, 61801, USA
[3] School of Biomedical Engineering, Korea University, Seoul, 02841, Republic of Korea.

Corresponding Author: Jahyun Koo (jahyunkoo@korea.ac.kr)

ABSTRACT

This article highlights new opportunities of inorganic semiconductor materials for bio-implantable electronics, as a subset of 'transient' technology defined by an ability to physically dissolve, chemically degrade, or disintegrate in a controlled manner. Concepts of foundational materials for this area of technology with historical background start with the dissolution chemistry and reaction kinetics associated with hydrolysis of nanoscale silicon surface as a function of temperature and pH level. The following section covers biocompatibility of silicon, including related other semiconductor materials. Recent transient demonstrations of components and device levels for bioresorbable implantation enable the future direction of the transient electronics, as temporary implanters and other medical devices that provide important diagnosis and precisely personalized therapies. A final section outlines recent bioresorbable applications for sensing various biophysical parameters, monitoring electrophysiological activities, and delivering therapeutic signals in a programmed manner.

1. INTRODUCTION

Recent advances in chemistry of the materials introduced unusual classes of electronic devices, which dissolve, disintegrate, or otherwise physically or chemically decompose in a defined period. Such types of "transient" materials and processes may enable eco-electronics that minimize electronic wastes or provide extremely high security devices that disappear physically for military uses or intellectual property rights, which makes data recovery impossible [1], [2]. Another interesting opportunity of 'transient' electronics is an application to implantable bio-devices that disappear harmlessly in the body dissolve in adjacent tissues. This technology, sometimes referred to as bioresorbable electronics, provides diagnostic or therapeutic function, and then disappears entirely to eliminate the need for surgical removal [3], [4].

Flexible electronics in the early 2000s brought many opportunities in the new class of electronics, such as wearable gears and epidermal sensors. In the inorganic materials field, at that time, they were developing ultra-thin inorganic materials in a nanoscale (~300 nm) for high performance flexible electronics due to its stable mechanical and chemical structures, compared to those of organic materials [5]. The research of thinning silicon (Si) semiconductor up to 200 nm encountered dissolvable characteristics of monocrystalline Si in the water [1]. The nanoscale forms of Si that hydrolyze in biofluids to yield biocompatible byproducts over biologically relevant timescales qualitatively advanced the field by providing direct routes to high performance operation [6]. When combined with bioresorbable conductors, dielectrics, substrates, and encapsulation layers, this nanoscale Si layer can provide the basis for a broad,
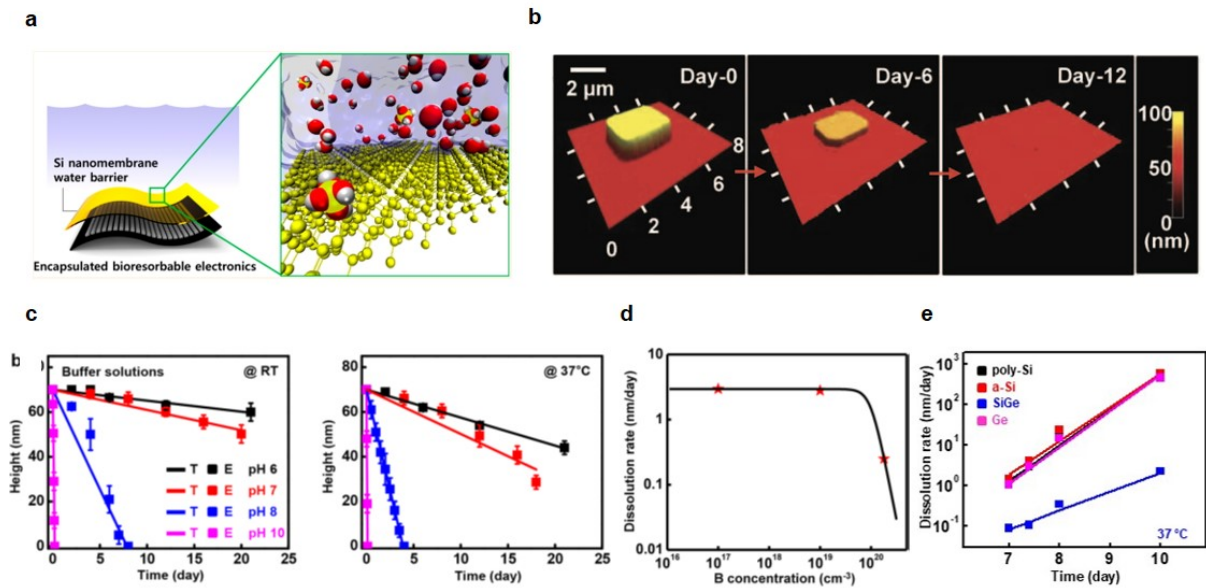
Figure 1. Chemistry and Kinetics of Si NM dissolution in various aqueous environments. (a) Schematic illustration of Si dissolution with reaction of water. (Reproduced with permission, 2017, ACS). (b) Series of topographical images of a Si NM during hydrolysis in p-PBS. (Reproduced with permission, 2012, AAAS). (c) Dissolution kinetics of a Si NM in buffer solutions with various pH at room temperature (left) and body temperature (right, 37 °C) expressed in thickness change. (Reproduced with permission, 2014, Wiley). (d) Dopant concentration dependent dissolution of a Si NM in phosphate buffer solution at 37 °C. (Reproduced with permission, 2014, ACS). (e) Dissolution kinetics of poly-Si, a-Si, SiGe, and Ge in buffer solution with different pH at 37 °C. Dissolution rates of a-Si, poly-Si, Ge, and SiGe are 4.1, 2.8, 3.1, 0.1 nm/day, respectively.22 (Reproduced with permission, 2015, ACS).

general class of bioresorbable electronic technology. Other properties of Si, such as its piezoresistivity and photovoltaic capacity, allow other types of bioresorbable devices such as implantable photodetectors, strain gauges and pH sensors [3]. Additional choices in semiconductors (silicon germanium (SiGe), zinc oxide (ZnO), synthetic polymers) also enable versatile applications [7]. The most advanced bioresorbable devices now exist as complete systems with successful demonstrations of clinically relevant modes of operation in animal models [3], [4], [8].

This article highlights the concepts of the foundational materials for this transient technology, starting with the dissolution chemistry and reaction kinetics associated with the hydrolysis of nanoscale Si layer (doping concentration, crystallinity) as a function of temperature and pH. The following discussion focuses on key supporting materials, including a range of dielectrics, metals, and substrates with exhaustive biocompatibility tests. A final section summarizes bioresorbable electronics for sensing various biophysical parameters, monitoring electrophysiological activities in a programmed manner.

2. DISSOLUTION CHEMISTRY OF SILICON NANOMATERIALS

Monocrystalline, electronic-grade Si is generally considered chemically stable in ambient, aqueous environments, due to the spontaneous formation of a native oxide on its surface. This notion of stability depends, however, on structural dimensions and on observational timescales. Specifically, loss of material from the surface of a bulk Si wafer (thickness of ~1 mm) immersed in water at rates of a few nanometers per day can, in most cases, be neglected over laboratory timescales; such rates of loss for Si nanowires, nanoribbons or nanomembranes will lead to their complete disappearance during similar timeframes [1]. In the context of systems described in this review, active silicon nanostructures dissolve in relevant aqueous environments within several days or weeks, depending on the geometry, the chemical termination of the silicon surface, the type and level of doping of the silicon and the composition and temperature of the surrounding solutions.

Previous studies of Si surfaces with water molecules suggest that the most important reaction is hydrolysis in water, which generates orthosilicic acid $(Si(OH)_4)$ and hydrogen as byproducts $(Si + 4H_2O \rightarrow Si(OH)_4 + 2H_2)$, as illustrated in Figure 1a. This chemical product $(Si(OH)_4)$ presents in natural and biological fluids in the body, commonly at concentrations between 100 to 101 ppm [9]. Dissolution of silicon nanomaterials, typically ranges with µg-scale in total mass for biomedical applications. Specifically, the combined use of Si nanomaterials with water-soluble dielectric and conductive materials offer many opportunities. Figure 1b shows the representative results of hydrolysis of Si nanostructure
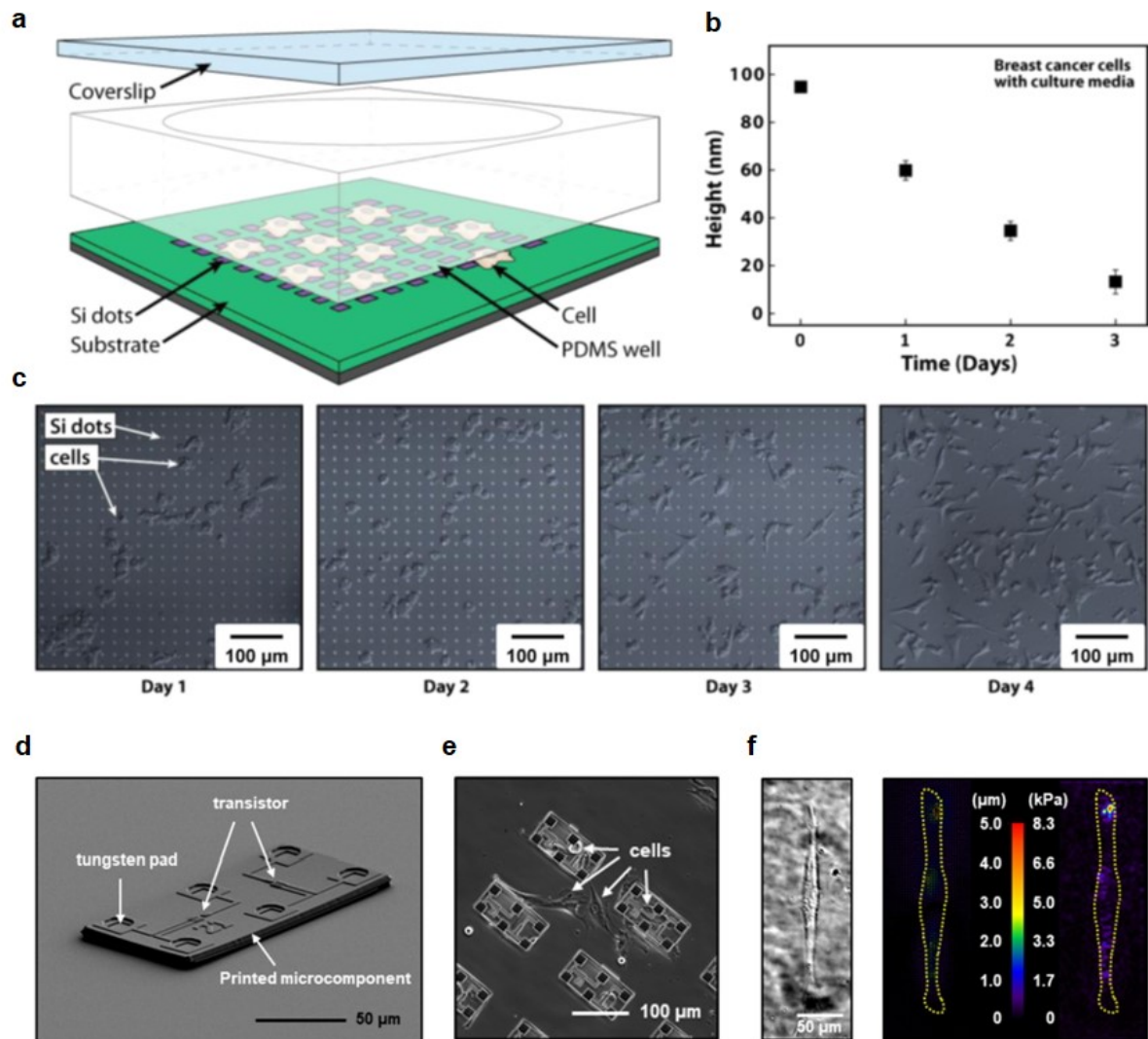
Figure 2. Biocompatibility of silicon nanomaterials. (a) Schematic illustration of *in vitro* cell culture evaluation for cytotoxicity and dissolution behaviors of Si nanostructure. Cells from a metastatic breast cancer cell line (MDA-MB-231) were cultured on a patterned Si nanostructure and solid substrate in a PDMS-based incubation chamber. (Reproduced with permission, 2014, ACS). (b) Measured change in thickness of the Si NMs characterized by AFM during the cell culture of the breast cancer cells with cultured media at 37 ℃. (Reproduced with permission, 2014, ACS). (c) Differential contrast images of the cell culture, illustrating the growth and proliferation trends of the cells in consecutive days in the conditioned environment in (b). The prolific trend of the viable cells, consistent with the data of (b), demonstrates the biocompatibility of the breast cancer cells until the complete dissolution of square Si NMs on the fourth day. (Reproduced with permission, 2014, ACS). (d) SEM image of p-channel metal-oxide-semiconductor field-effect transistors (MOSFETs) fabricated from commercial foundry (X-Fab Semiconductor Foundries) thin films exemplified by Si, SiNx, SiO$_2$, Ti/TiN, and W. (Reproduced with permission, 2018, ACS) (e) Phase-contrast image of in vitro studies of biocompatibility test of such microcomponents arrays of transistors shown in (d). CCD18 cells with a density of 5000 cells/cm^2 incubated on the devices at 37 ℃ and humidified atmosphere with 5% CO$_2$ for 18 h of culture exhibit a trend to adhere to the surface structures by topological effects. The phase-contrast image was taken in situ, where trypan blue treatment (Sigma-Aldrich) established imaging of cell nuclei. (Reproduced with permission, 2018, ACS). (f) TFM images of displacement and stress fields of a representative cell incubated on the transistor arrays with conditioned microenvironment over 18 h. The traction-induced displacements of the extracellular matrix corresponding with the metabolic reactions of cells to the surrounding stimuli indicate the cell's tonicity. (Reproduced with permission, 2018, ACS).

(3 μm×3 μm×70 nm, p-type, 10-20 Ω·cm) in simulated biofluid (phosphate buffered saline, pH 7.4, 37 ∘C). Here, the dissolution rate is ~5 nm/day, which results in the complete disappearance of this nanoscale Si within 12-13 days [1]. Figure 1c summarizes the dependence of the reaction rate on the pH level from 6 to 14. Results from the high pH part of this range connect to the well-established kinetics of etching and micromachining of bulk silicon in alkaline solutions. The linear dependence of the thickness (h) on reaction time indicates that the chemistry involves surface erosion, without a significant contribution from reactive diffusion of water into the silicon. As a result, the simple expression h=h0-Rt, where h0 and R are the initial thickness and the reaction rate, respectively, captures the behaviors.
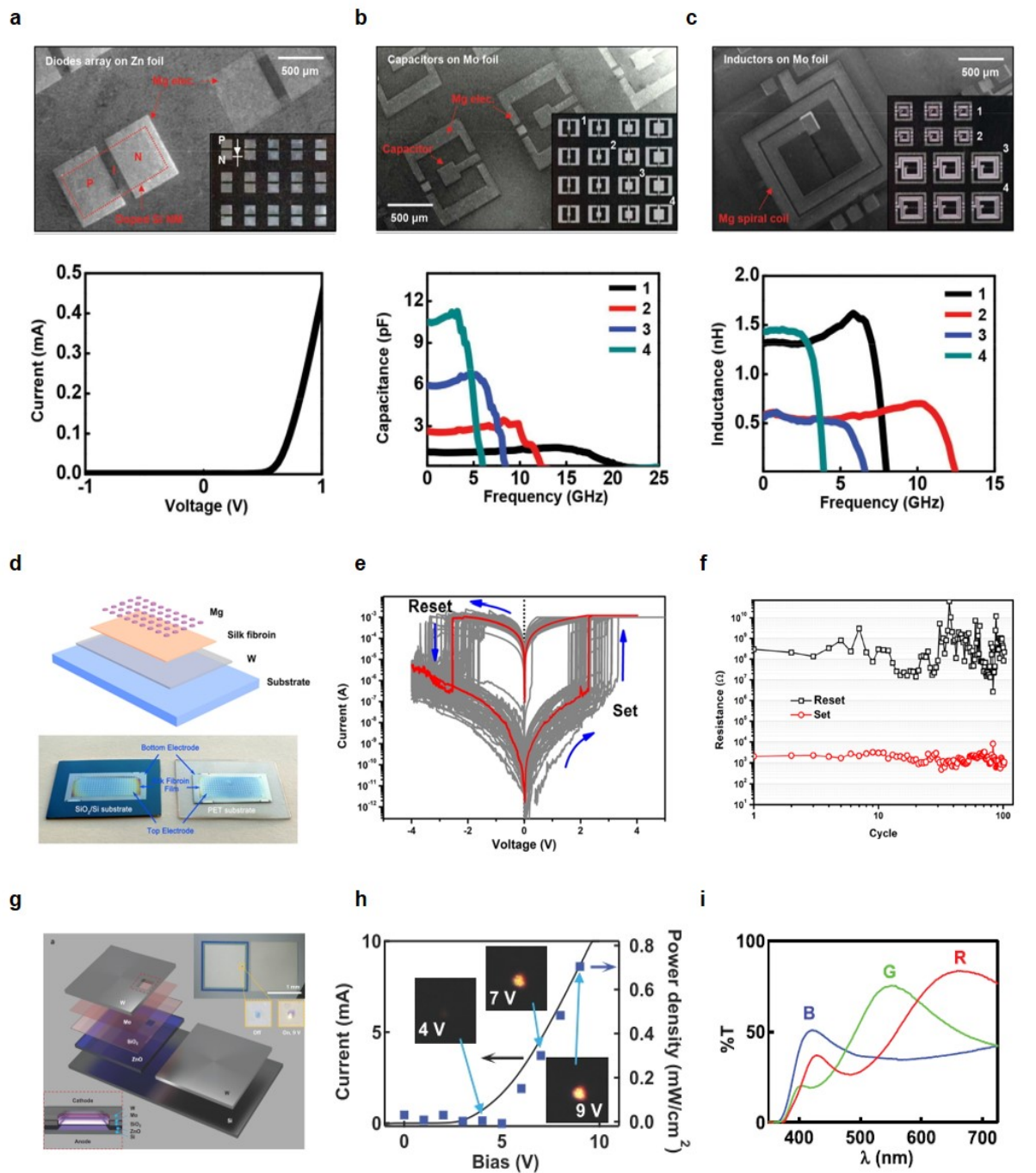
Figure 3. Demonstration of transient electronic devices on various biodegradable metal foil substrates. (a) Scanning electron microscope (SEM) and optical microscope image (inset) of an array transient PIN diode on a Zn foil (~10 μm thick) observed by SEM and optical microscope (up and inset). Current–voltage characteristics are typical of PIN diodes (bottom). (Reproduced with permission, 2015, ACS). (b) SEM and optical images of capacitors with different sizes, built using Mg electrodes (top/bottom) and PECVD SiO_2 dielectrics on Mo foil (~10 μm thick) (up). Measured capacitance as a function of frequency up to ~25 GHz. (Reproduced with permission, 2015, ACS). (c) SEM and microscope images (inset) of planar spiral coils on a Mo foil substrate (~10 μm) (up). Mg layers provide bottom (~300 nm) and top (~3.5 μm) electrodes, and a PECVD SiO_2 layer (~900 nm) serves as interlayer dielectric. Inductance as a function of frequency from 0 to 15 GHz (right). (Reproduced with permission, 2015, ACS). (d-f) Metal-insulator-metal structure to demonstrate a resistive memory device, in which W and Mg serve as inert and active electrodes, respectively. (Reproduced with permission, 2018, ACS). (g-i) Structure and optical properties of fully transient LEDs with oxygen vacancy doped n-type ZnO(001) films deposited on n-type Si(111) substrates by pulsed laser deposition. (Reproduced with permission, 2019, Wiley).

The biochemical complexity increases considerably upon the introduction of ions into the surrounding aqueous solutions. Certain ions significantly accelerate the rates of reaction [10], including those (e.g. Na^+, Ca^{2+}, Mg^{2+} cations and Cl^-, HCO_3^-, HPO_4^- anions) that are common in environmental and

Table 1. Summary of biocompatibility test

*Si NM=silicon nanomembrane, a-Si=amorphous crystalline silicon, Mono-Si=monocrystalline silicon, PLGA= poly(lactic-co-glycolic acid).

	Hwang et al. [6]	S. Kang et al. [14]	Hwang et al. [6]	K. J. Yu [4]	Hwang et al. [1]	S. Kang et al. [3]
	Cell test		**Animal test**			
Materials	Si NM	Poly Si, a-Si, SiGe, Ge, Mono-Si	Si NM, Mg, MgO	Si NM, SiO_2, Si_3N_4, Mo, PLGA	Si NM, Mg, MgO/SiO_2, silk	Porous Si, Si NM, PLGA, SiO_2, polyanhydride
Device structure & test setup	Dot patterned Si NM	Dot patterns of materials.	Si NM, Mg,MgO on silk substrate	MOSFETs: 100 µg of Mo, 1.43 µg of Si, 306 µg of SiO_2, 264 µg of Si_3N_4, and 27 pg of P	Mg/MgO inductor, Mg/MgO capacitor, Si NM/MgO/Mg transistor, Si diode, Mg resistor on silk substrate	Si NM piezo resistive sensor
Biocompatibility model	Breast cancer cell line (MDA-MB-231) (cell density: 300 cells/mm^2)	Mouse fibroblast cell (L929) viability for 7 days (cell density: 300 cells/mm^2).	Subdermal region of mice with Si NM, Mg, MgO on silk substrate	Rat brain tissue	Implantation in subcutaneous tissue for 2 weeks	Rat brain tissue for 2, 4, 8 weeks
Biocompatibility results	The cell viability on 1, 5, and 10 days show no difference	>95% relative viability of all cells exposed to 75% and 100% extracted supernatants, respectively	No cytotoxicity was observed by immunoprofiling using primary immune cells from the axillary and branchial draining lymph nodes.	No significant astrogliosis is noted at distant sites within the ipsilateral hemisphere	No inflammation reaction	No overt immune reaction to the device and its by-products

biological fluids at concentrations from 0.1 to > 50 g/L. In the case of low ionic concentration, the Si nanomaterials exhibit comparably low dissolution rate at ~1 nm/day (e.g. 0.05 M K_2HPO_4/KH_2PO_4), while the rate increases to 65 nm/day in high ion concentrations (e.g. 1 M K_2HPO_4/KH_2PO_4). These variations arise from catalyzing effects of the ions, as suggested by density functional theory (DFT) for the case of anions (HPO_4^{2-} or Cl^-) where interactions with surface Si atoms can weaken nearby Si-Si backbonds [10].

The rates of dissolution of nanoscale Si with boron (p-type) dopants at concentrations from 10^{17} cm^{-3} to 10^{20} cm^{-3} in simulated biofluid (phosphate buffer solution, 0.1 M, pH 7.4) show that the dopants in the silicon also affect the reaction chemistry (Figure 1d). The dissolution rates remain the same for concentrations up to 10^{19} cm^{-3}, and then decrease significantly at 10^{20} cm^{-3} with similar behavior resulting from doping with phosphorus (n-type) [11]. Such effects are well known in silicon KOH (10-57%) etching process with different quality of the native oxide layer during the doping procedure [12,13]. Specifically, measurements of ellipsometry show dense layers (~1 nm) of SiO_2 on highly doped Si (either boron or phosphorous) when immersed in water, possibly due to barrier-less oxidation pathways facilitated by the presence of dopants or lattice strains induced by the different atomic sizes of Si and dopants [12], [13]. On the other hand, lightly doped Si exhibits

porous surface layers of SiO_2 that grow in parallel with the dissolution of Si. The rate of dissolution of SiO2 is much slower than that of Si, thereby providing a plausible chemical explanation for the variation in rate with the doping level.

The crystallinity of Si affects the dissolution rate in water [14]. For example, polycrystalline (poly-Si) and amorphous (a-Si) silicon are useful as active materials in thin solar cells and photodetectors; silicon germanium (SiGe) enables high-speed transistors. Figure 1e summarizes the dissolution kinetics of poly-Si, a-Si, Ge, and SiGe in phosphate buffer solution (pH 7.4, 0.1 M, 37 ◦C).

3. OTHER BIORESORBABLE ELECTRONIC MATERIALS

Recent works show that magnesium (Mg), zinc (Zn), tungsten (W), and molybdenum (Mo) can serve as bioresorbable metals; systematic studies presents their dissolution behavior in thin-films and foils [15,16]. These metals react with water, according to: $Mg + 2H_2O \rightarrow Mg(OH)_2 + H_2$, $Zn + 2H_2O \rightarrow Zn(OH)_2 + H_2$, $2W + 2H_2O + 3O_2 \rightarrow 2H_2WO_4$, $2Mo + 2H_2O + 3O_2 \rightarrow 2H_2MoO_4$. Metallic alloys of these metals can be a possible option of tunable dissolution of transient electronics, such as AZ31B (Mg-Zn alloy). The dissolution rates of these metals and metal alloys (Mg, Zn, W, Mo, AZ31B) in a representative biofluid
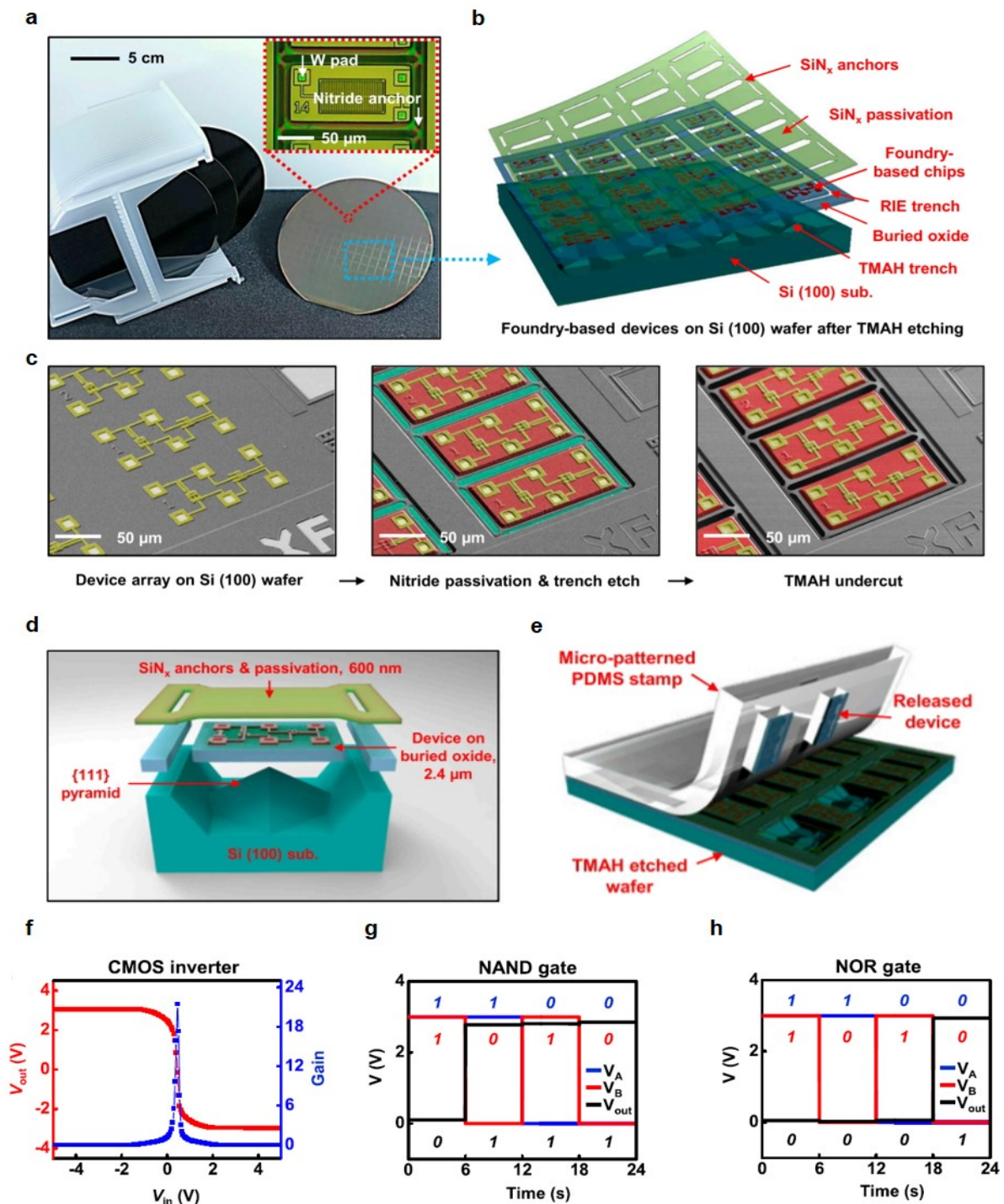
Figure 4. Wafer-scale release of foundry-based, ultrathin silicon components for transient electronics. (a) Photograph of fully processed wafers. (Inset) Magnified view that shows the releasable configuration of a representative device in this foundry-based platform. (b) Schematic illustration of such device arrays after undercut release by TMAH anisotropic etching. (c) SEM images of key processing steps for release. The colorized regions correspond to the device array (gold), the released region of individual device blocks (red), and the underlying silicon (100) handle wafer (cyan). The individual frames correspond to the unprocessed wafer (Left), the wafer after passivation and trench etching (Center), and the wafer after TMAH undercut etching (Right), respectively. (d) Aspects of release of thin, transient CMOS devices based on anisotropic etching of the Si (100) handle wafer. (e) Schematic illustration of the process for transfer printing with a PDMS stamp. Output voltage characteristics of a CMOS inverter (f), a NAND gate (g), and a NOR gate (h). The supply voltage is 3 V. V_{in}, input voltage. (Reproduced with permission, 2017, United States National Academy of Sciences).

(Hank's solution) are 7×10^{-2}, 7×10^{-3}, $1.7 \sim 0.3\times10^{-3}$, 3×10^{-4}, 2×10^{-2} µm h^{-1} at room temperature, respectively [16].

4. BIOCOMPATIBILITY OF SI NANOMATERIALS

The biocompatibility of Si nanomaterials and their byproducts of hydrolysis are critically important for biomedical applications. Figure 2a shows the typical poly(dimethylsiloxane) (PDMS)-based micro-incubation setup for *in vitro* assessment of the cytotoxicity. A patterned array of Si nanostructures dissolves in the PDMS well structure to allow the measurement of changes in the thicknesses of the Si nanostructure (Figure 2b). The arrays of square Si nanomaterials were no longer visible on the fourth day, indicating Si fully dissolved without significant cell death (Figure 2c). The main product, silicic acid, is a nontoxic small molecule that represents the most common form of bioavailable Si in the human body (serum contains 11–25 μg silicon/dL) [17]. The silicic acid does not accumulate within the body, but is absorbed by the adjacent tissue and is eliminated via the urinary pathway [18]. Separate studies of the biocompatibility of Si nanomaterials support similar conclusions [1], [3], [4], [6], [14]. Table 1 summarizes the representative results of bioresorbable materials or their combination of implantable device level. Hwang *et al.*[6] utilized metastatic breast cancer cell line (MDA-MB-231)) and reported viability remains above 93% throughout the complete dissolution process, showing no significant cell toxicity. Kang *et al.*[3] used mouse fibroblast cell (L929), showing >95% relative viability of all cells with no significant changes in the percentage of early or late apoptosis.

Analysis of mechanotransduction via traction force microscopy (TFM) can offer quantitate and direct monitoring of cellular activities [19]. Figure 2d highlights the microstructure of p-channel metal-oxide-semiconductor field-effect transistors (MOSFETs). As shown in Figure 2e, CCD18 cells incubated at 37 °C tend to adhere along structural features following previously reported topology effects. TFM analysis of CCD18 human colon fibroblasts cell represents the 10 mM concentration of silicic acid, which does not show cell toxicity without significant difference between groups (Figure 2f).

Animal model studies also support similar results of the cell cytotoxicity test. Si nanomaterials on silk substrates, as subdermal implants in mice, indicate no change of body weight and no additional generation of primary immune cells from the axillary and branchial draining lymph nodes [11]. Related biocompatibility studies involve Si nanomaterials with other transient materials, such as Mg, SiO_2 and PLGA in the form of functional devices. In one case, pressure sensors implanted into the intracranial space of rat models for 2, 4, and 8 weeks, indicated no overt reactions of brain glial cells, and no focal aggregation of glial cells [3]. Astrocytosis (an increase in the number of astrocyte cells) and microglial activity at the cortical surface remain within normal limits, indicating a minimal immune reaction to the device or its byproducts [3]. Immunohistology of thin, flexible electronic systems for electrophysiological mapping on the surface of the brain indicates no significant astrogliosis and no microglial reaction throughout the functional lifetime of the device and its complete dissolution [4].

5. DEMONSTRATION IN THE TRANSIENT COMPONENTS AND DEVICES

Transient metal substrate offers robust, compatible with most commercial microelectromechanical system (MEMS) fabrication process, and thermally and chemically stable ways to build transient components. Figure 3a-c illustrates diodes, capacitor, and inductor on the biodegradable metal foils, such as Fe, Mo, W, and Zn (~10 μm thick). Nanoscale Si layer (~200 nm thick) with Mg electrodes (~300 nm thick) on a Zn foil (~10 μm thick) consists of an array of PIN diodes (Figure 3a, up), and shows typical electrical characteristics (Figure 3a, bottom). Capacitors (Figure 3b) and inductors (Figure 3c) are also possible. Parallel-plate capacitors of various lateral dimensions (left, black, 150 × 150 μm; red, 250 × 250 μm; blue, 400 × 400 μm; green, 550 × 550 μm) can be formed with SiO_2 (~900 nm thick) as the dielectric and Mg as the electrodes on Mo foils (~10 μm). Capacitances (Figure 3b, bottom) in the frequency range between 0 and 25 GHz. Spiral inductors with two or three turns (Figure 3c) constructed using Mg traces for the electrodes and SiO_2 (~900 nm thick) as the interlayer dielectric can be formed on Mo foils (~10 μm thick). Transient resistive memory and light-emitting diodes (LEDs) constructed with semiconductors and transient electrode are also possible. Figure 3d illustrates metal-insulator-metal structure to demonstrate a resistive memory device, in which W and Mg serve as inert and active electrodes, respectively, and silk fibroin film serves as the switching layer [20]. Figure 3e shows the I−V curves of a W/silk fibroin/Mg sandwich structure with swiped voltage from -4 to 4 V. The I−V characteristic after electroforming exhibits a typical bipolar resistive switching behavior. The narrow distributions of set voltage and reset voltage indicate versatility of the device. Reversible switching without degradation up to 100 cycles demonstrates possible transient memory application, as shown in Figure 3f. Figure 3g describes the structure of fully transient LEDs with oxygen vacancy doped n-type ZnO(001) films deposited on n-type Si(111) substrates by pulsed laser deposition. The threshold voltage of the ZnO LED is ~5 V, as observed in the optical power density–current–voltage (L–I–V) curve (Figure 3h), similar to typical ZnO p–n junction LEDs [21], 22]. The feature of broadband emission allows fabrication of red (R), green-yellow (G), and blue-violet (B) LEDs by the

addition of transient Fabry–Perot optical filters (Figure 3i).

6. FOUNDRY-COMPATIBLE APPROACHES FOR TRANSIENT ELETRONICS

The efforts of foundry-based approaches for transient electronics can provide high potential to serve as the manufacturing basis for bioresorbable and implantable devices. For example, the recent portfolio of biodegradable materials, such as Si, SiO_2, and W, with only minute amounts of nondegradable materials (Ti/TiN) allows transient CMOS fabrication [23]. X-FAB Semiconductor Foundries, which uses 1-µm design rules [24], [25], enable capacitors, p-channel and n-channel transistors on a 6-inch wafer, as shown in Figure 4a. The prepared transient components can be transfer-printed from 6-inch wafer after undercut release by TMAH anisotropic etching (Figure 4b). As illustrated in Figure 4c, the procedure for release from the underlying substrate exploits lithographically defined structures and anisotropic wet chemical etching, with the BOX as a back-surface etch stop. Careful control, combined with optimized procedures for transfer printing, can lead to cumulative yields of greater than 99%. Schematic illustrations and SEM images of the undercut profiles appear in Figure 4d. The results are consistent with etching that proceeds in the Si <110> direction, bounded by (111) planes. By consequence, an undercut process that begins at the RIE trenches leaves {111} silicon pyramids positioned at the centers of the device blocks [23], [26] The transfer printing process uses stamps of PDMS with relief features defined to manipulate one device at a time or large collections of them simultaneously (Figure 4e). Figure 4f-h show output voltage characteristics for a CMOS inverter (Figure 4f), a negative-AND (NAND) (Figure 4g), and a negative-OR (NOR) (Figure 4h) circuit obtained in this manner. For the inverter, the voltage transfer characteristics exhibit gains of up to ~21 at supply bias levels of ±3 V, with input low voltage (VIL) of 0.05 V and input high voltage (VIH) of 0.85 V, that are capable of a large noise margin for high noise immunity.

7. BIORESORBABLE ELECTRONIC IMPLANTS

Implantable devices offer diverse and essential functions for research, advanced diagnosis, and treatment. In certain cases, this function is most valuable for finite operation time, matched to intrinsic biological processes, such as wound healing. Here, removal of the devices after this operation time is required to eliminate the unnecessary load on the patient, and the associated risks of uncontrolled migration within the body, pathological tissue responses and infection. The surgical retrieval procedures, however, can involve complications themselves. Transient, bioresorbable electronics offer a potential solution in this context. The following summarizes recent research demonstrations.

Figure 5a shows a bioresorbable sensor of intracranial pressure, designed for monitoring recovery following a traumatic injury to the brain. The device incorporates a Si NM piezoresistive strain sensor integrated onto a flexible PLGA membrane that forms the top seal of an underlying cavity created on the etched region of the surface of a nanoscale Si substrate or Mg foil [3]. Changes in the pressure of surrounding fluids induce deflections of the membrane and changes in the resistance of the strain gauges, for electrical readout. Figure 5b illustrates its application as an intracranial pressure monitor with an interface to a wireless unit for data transmission. Here, degradable wires coated with bioresorbable polymers provide electrical connections between the sensor and external electronics. Studies using a rodent model indicate the stable measurement of temperature and pressure in the intracranial space for three days, and complete bioresorption within 4-6 weeks in biofluids at 37 ∘C [3].

Active electronic interfaces to the brain also have utility in this context of monitoring during recovery from an injury. Figure 5c shows passively and actively addressed systems for electrophysiological monitoring on the surface of the brain, where the constituent materials and fabrication strategies are similar to those for the devices in Figure 5a [4]. In these platforms, Si NM electrodes record normal physiologic and epileptiform activity such as electrocorticography (ECoG) and subdermal encephalograms (EEG), both in acute and chronic situations. Here, high doping levels in the Si electrodes lead to relatively slow rates of dissolution in biofluids, thereby enabling use for over 33 days. In addition to monitoring, bioresorbable electronic systems can also be utilized in various therapy modes [8]. For example, bi-layered radio frequency coils, built by patterned Mg film (~50 µm thick) and integrated with Si diodes (PIN diode, 200 nm thick), Mg capacitor (Mg/SiO_2/Mg = 50-µm/600-nm/50-µm) can deliver therapeutic stimulation signal (20 Hz, monophasic pulsed wave) to the sciatic nerve in a rat model. The Mg coils, wirelessly powered by RF, allow full implantation in a back of rat, and the extended electrode can reach the target tissue (sciatic nerve), as shown in Figure 5e. The constituent materials completely disintegrate and dissolve within a month. Minimal inflammatory responses and fibrosis occur over an eight-week monitoring period, with no evidence of axonal injury or damage at the nerve-cuff interface. The application in the transected injured animal group shows enhanced therapeutic effects, such as increased muscle function reaction by measuring electromyography (EMG) signal. Furthermore, the
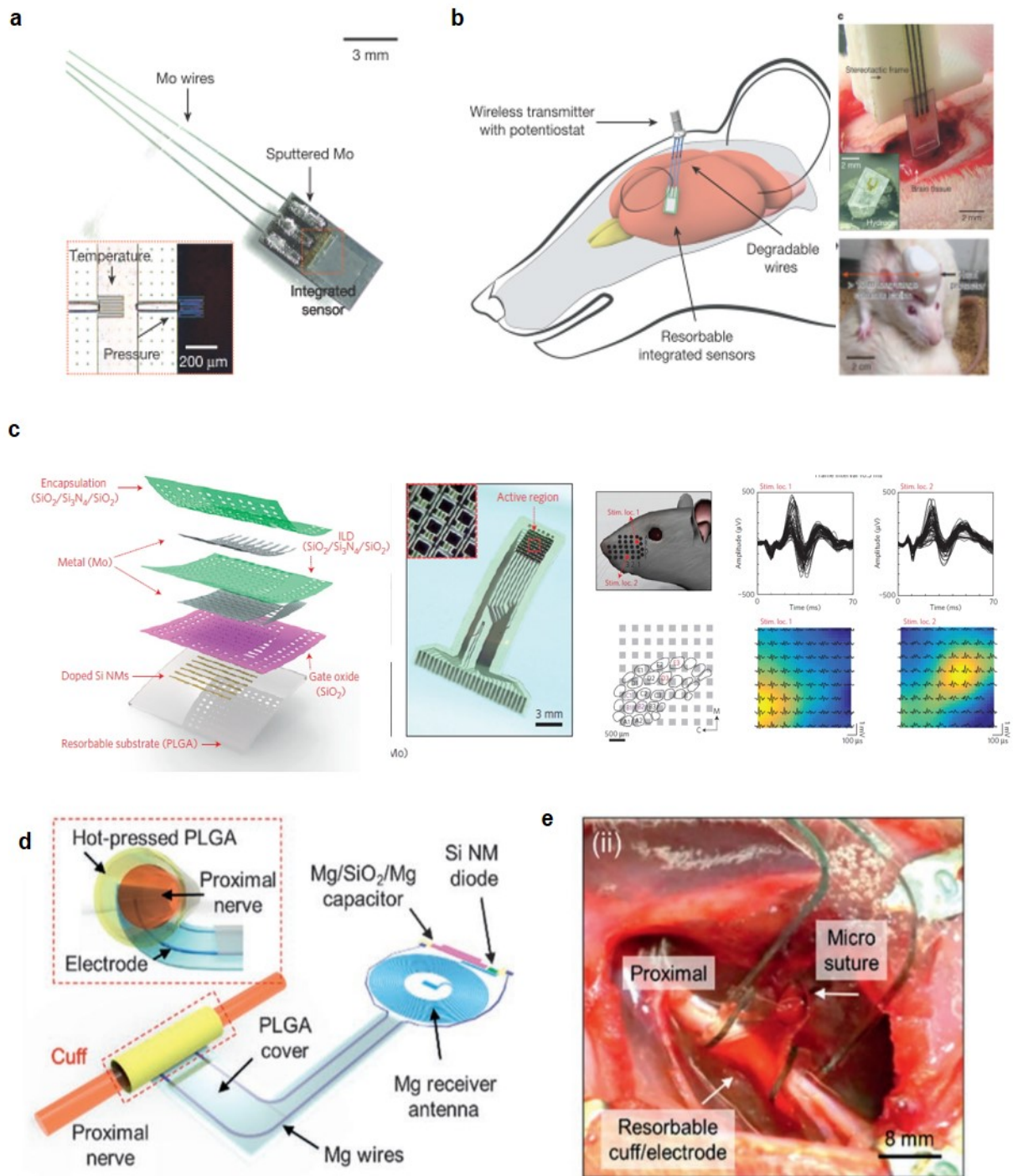
Figure 5. Biomedical applications of bioresorbable devices level. (a) Image of bioresorbable pressure and temperature sensors integrated with dissolvable metal (Mo) interconnects. (Reproduced with permission, 2016, Nature Publishing Group). (b) Diagram of a bioresorbable temperature and pressure sensor in the intracranial space of a rat model (left). Injectable form of pressure sensor for deep brain monitor (right, upper). Wireless operation of pressure sensor with percutaneous wiring (right, lower). (Reproduced with permission, 2016, Nature Publishing Group) (c) Structure and image of a bioresorbable actively multiplexed sensing system. (Reproduced with permission, 2016, Nature Publishing Group). (d) Image of nerve stimulator integrated with bioresorbable PLGA cuff electrode. (Reproduced with permission, 2018, Nature Publishing Group). (e) Schematic illustration of application at the peripheral nerve interface. (Reproduced with permission, 2018, Nature Publishing Group).

modified versions of this same platform can address a range of clinical scenarios and target tissues/organ systems, including the brain and spinal cord, skeletal muscles, and cardiac tissues with relatively few modifications to the form factor and the interfacial electrode sites.

8. SUMMARY AND PERSPECTIVE

Insights from the chemistry of dissolvable semiconductor materials open bioresorbable classes of electronics, with broad potential utility in eco-electronics, military or industrial secure data management, and temporary implantable medical systems. The other materials in these platforms are equally important, and they offer many potential fields of research for future development in materials, fabrications, device design, where high performance operation in sensing, actuation, and power harvesting. Additional opportunities lie in the development of passive, as well as actively stimulated, packaging materials, thereby allowing precisely controlled lifetimes of devices with a wide range of clinical options. The possible research directions, from fundamental studies of the semiconductor fabrication and surface chemistry to innovative engineering of the devices and systems, and the important potential applications in biomedicine suggest the future for this field.

ACKNOWLEDGMENT

AUTHOR CONTRIBUTIONS

The manuscript was written through contributions of all authors.

REFERENCES

[1] S.-W. Hwang, H. Tao, D.-H. Kim, H. Cheng, J.-K. Song, E. Rill, M.A. Brenckle, B. Panilaitis, S.M. Won, Y.-S. Kim, Y.M. Song, K.J. Yu, A. Ameen, R. Li, Y. Su, M. Yang, D.L. Kaplan, M.R. Zakin, M.J. Slepian, Y. Huang, F.G. Omenetto, J.A. Rogers. (2012, Sep.). A Physically Transient Form of Silicon Electronics. *Science.* [Online]. 337(6102), pp. 1640-1644.

[2] S.-W. Hwang, G. Park, H. Cheng, J.-K. Song, S.-K. Kang. (2014, Apr.). 25th Anniversary Article: Materials for High-Performance Biodegradable Semiconductor Devices. *Adv. Mater.* [Online]. 26, pp. 1992-2000.

[3] S.-K. Kang, R. K. J. Murphy, S.-W. Hwang, S. M. Lee, D. V. Harburg. (2016, Feb.). Bioresorbable Silicon Electronic Sensors for the Brain. *Nat.* [Online]. 530, pp. 71-76.

[4] K. J. Yu, D. Kuzum, S.-W. Hwang, B. H. Kim, H. Juul. (2016, Jul.). Bioresorbable Silicon Electronics for Transient Spatiotemporal Mapping of Electrical Activity from the Cerebral Cortex. *Nat. Mat.* [Online]. 15, pp. 782-791.

[5] J. A. Rogers, M. G. Lagally & R. G. Nuzzo. (2011, Sep.). Synthesis, assembly and applications of semiconductor nanomembranes. *Nat.* [Online]. 477(7362), pp. 45-53.

[6] S.-W. Hwang, G. Park, C. Edwards, E.A. Corbin, S.-K. Kang, H. Cheng, J.-K. Song, J.-H. Kim, S. Yu, J. Ng, J.E. Lee, J. Kim, C. Yee, B. Bhaduri, Y. Su, F.G. Omennetto, Y. Huang, R. Bashir, L. Goddard, G. Popescu, K.-M. Lee. (2014, Mar.). Dissolution Chemistry and Biocompatibility of Single-Crystalline Silicon Nanomembranes and Associated Materials for Transient Electronics. *ACS Nano.* [Online]. 8(6), pp. 5843-5851.

[7] D. Lu, T.-L. Liu, J.-K. Chang, D. Peng, Y. Zhang, J. Shin, T. Hang, W. Bai, Q. Yang, J.A. Rogers. (2019, Sep.). Transient Light-Emitting Diodes Constructed from Semiconductors and Transparent Conductors that Biodegrade Under Physiological Conditions. *Adv. Mater.* [Online]. 31(42), 1902739.

[8] J. Koo, M.R. MacEwan, S.-K. Kang, S.M. Wong, M. Stephen, P. Gamble, Z. Xie, Y. Yan, Y.-Y. Chen, J. Shin, N. Birenbaum, S. Chung, S.B. Kim, J. Khalifeh, D.V. Harburg, K. Bean, M. Paskett, J. Kim, Z.S. Zhony, S.M. Lee, R. Zhang, K. Luo, B. Ji, A. Banks, H.M. Lee, Y. Huang, W.Z. Ray, J.A. Rogers. (2018, Dec.) Wireless bioresorbable electronic system enables sustained nonpharmacological neuroregenerative therapy. *Nature Medicine.* [Online]. 24, pp. 1830-1836.

[9] S.-K. Kang, J. Koo, Y.K. Lee, J.A. Rogers. (2018, Apr.). Advanced Materials and Devices for Bioresorbable Electronics. *Acc. Chem. Res.* [Online]. 51(5), pp. 988-998.

[10] L. Yin, A.B. Farimani, K. Min, N. Vishal, J. Lam, Y.K. Lee, N.R. Aluru, J.A. Rogers. (2015, Jan.). Mechanisms for Hydrolysis of Silicon Nanomembranes as Used in Bioresorbable Electronics. *Adv. Mat.* [Online]. 27(11), pp. 1857-1864.

[11] S.-W. Hwang, G. Park, C. Edwards, E.A. Corbin, S.-K. Kang. (2014, Mar.). Dissolution Chemistry and Biocompatibility of Single-Crystalline Silicon Nanomembranes and Associated Materials for Transient Electronics. *ACS Nano.* [Online]. 8(6), pp. 5843-5851.

[12] E.D. Palik, V.M. Bermudez, O.J. Glembocki. (1985, Jan.). Ellipsometric Study of the Etch-Stop Mechanism in Heavily Doped Silicon. *J. Eletrochem. Soc.* [Online]. 132(1), pp.135-141.

[13] M. Morita, T. Ohmi, E. Hasegawa, M. Kawakami, M. Ohwada. (1990, Mar.). Growth of native oxide on a silicon surface. *J. Appl. Phys.* [Online]. 68, pp. 1272-1281.

[14] S.-K. Kang, G. Park, K. Kim, S.-W. Hwang, H. Cheng, J. Shin, S. Chung, M. Kim, L. Yin, J.C. Lee, K.-M. Lee, J.A. Rogers. (2015, Apr.). Dissolution Chemistry and Biocompatibility of Silicon- and Germanium-Based Semiconductors for Transient Electronics. *ACS Appl. Mater. Interfaces.* [Online]. 7(17), pp. 9297-9305.

[15] S.-K. Kang, S.-W. Hwang, S. Yu, J.-H. Seo, E.A. Corbin, J. Shin, D.S. Wie, R. Bashir, Z. Ma, J.A. Rogers. (2015, Jan.). Biodegradable Thin Metal Foils and Spin-On Glass Materials for Transient Electronics. *Adv. Funct. Mater.* [Online]. 25(12), pp. 1789-1797.

[16] L. Yin, H. Cheng, S. Mao, R. Haasch, Y. Liu, X. Xie, S.-W. Hwang, H. Jain, S.-K. Kang, Y. Su, R. Li, Y. Huang, J.A. Rogers. (2013, Sep.). Dissolvable Metals for Transient Electronics. *Adv. Funct. Mater.* [Online]. 24(5), pp. 645-658.

[17] E.M. Carlisle. (1982, Jul.). The Nutritional Essentiality of Silicon. *Nutr. Rev.* [Online]. 40(7), pp. 193-198.

[18] J.G. Archibald, H. Fenner. (1957, Jun.). Silicon in Cow's Milk. *Int. J. Dairy Sci.* [Online]. 40(6), pp. 703-706.

[19] J.-K. Chang, M.A.B. Emon, C.-S. Li, Q. Yang, H.-P. Chang, Z. Yang, C.-I. Wu, M.T. Saif, J.A. Rogers. (2018, Aug.). Cytotoxicity and in Vitro Degradation Kinetics of Foundry-Compatible Semiconductor Nanomembranes and Electronic Microcomponents. *ACS Nano.* [Online]. 12(10), pp. 9721-9732.

[20] X. Ji, L. Song, S. Zhong, Y. Jiang, K.G. Lim, C. Wang, R. Zhao. (2018, Jun.). Biodegradable and Flexible Resistive Memory for Transient Electronics. *J. Phys. Chem. C.* [Online]. 122(29), pp. 16909-16915.

[21] A. Tsukazaki, A. Ohtomo, T. Onuma, M. Ohtani, T. Makino, M. Sumiya, K. Ohtani, S. F. Chichibu, S. Fuke, Y. Segawa, H. Ohno, H. Koinuma, M. Kawasaki. (2004, Dec.). Repeated temperature modulation epitaxy for p-type doping and light-emitting diode based on ZnO. *Nat. Mater.* [Online]. 4(1), pp. 42-46.

[22] A. Tsukazaki, M. Kubota, A. Ohtomo, T. Onuma, K. Ohtani, H. Ohno, S. F. Chichibu, M. Kawasaki. (2005, May). Blue Light-Emitting Diode Based on ZnO. *Jpn. J. Appl. Phys.* [Online]. 44, L643.

[23] J.-K. Chang, H. Fang, C.A. Bower, E. Song, X. Yu, J.A. Rogers. (2017, Jun.). Materials and processing approaches for foundry-compatible transient electronics. *Proc. Natl. Acad. Sci. U.S.A.* [Online]. 114(28), pp. E5522-E5529.

[24] S. Riches, C. Johnston. (2015, May). Electronics design, assembly and reliability for high temperature applications. 2015 IEEE International Symposium on Circuits and Systems.

[Online]. pp. 1158-1161.

[25] M.-A. Paun, F. Udrea. (2016, Feb.). Investigation into the capabilities of Hall cells integrated in a non-fully depleted SOI CMOS technological process. *Sens. Actuator A Phys.* [Online]. 242, pp. 43-49.

[26] L.M. Landsberger, S. Naseh, M. Kahrizi, M. Paranjape. (1996, Jun.). On hillocks generated during anisotropic etching of Si in TMAH. *J. Microelectromech. Syst.* [Online]. 5, pp. 106-116.

AUTHOR BIOGRAPHIES

Min-Ho Seo received his B.S. degree (Magna cum laude, 2011) in nanomechatronics engineering from Pusan National University and received his M.S. and Ph.D. degrees (2013 and 2018, respectively) in electrical engineering from the Korea Advanced Institute of Science and Technology (KAIST). From 2018 to 2019, he was a postdoctoral research fellow at the Information and Electronics Research Institute at KAIST. Since 2019, he started a postdoctoral researcher in the Center for Bio-integrated Electronics (CBIE) at Northwestern University in the United States. His research interests include nano/microelectromechanical systems (N/MEMS), biomedical electronics, bioresorbable electronics, flexible electronics, and physical and chemical sensor electronics. Seo can be reached by email at minho.seo@northwestern.edu

Seongbin Jo is studying for a B.S. degree in Chemical and Biomolecular Engineering from University of Illinois at Urbana-Champaign, USA (2014-2020). He is currently working for research internship in the School of Biomedical Engineering at Korea University. His research interests include biomedical transient electronics and implantable devices. Jo can be reached by email at sjo22@illinois.edu.

Jahyun Koo is currently an assistant professor in the School of Biomedical Engineering at Korea University. He received his BS and MS degrees in nuclear and quantum engineering from the Korea Advanced Institute of Science and Technology (KAIST), Republic of Korea, in 2010 and 2012, respectively. He received his PhD degree in materials science and engineering from KAIST in 2017. He was a postdoctoral researcher in the Center for Bio-Integrated Electronics at Northwestern University, USA (2017-2019). He was a visiting scholar in the Materials Research Lab at University of Illinois at Urbana-Champaign, USA (2015-2016). Koo can be reached by email at jahyunkoo@korea.ac.kr.